Mapping of the optical frequency comb to the atom-velocity comb

T. Ban, D. Aumiler, H. Skenderović, and G. Pichler
Institute of Physics, Bijenička 46, Zagreb, Croatia
(Received 20 December 2005; published 11 April 2006)

A mode-locked femtosecond laser is used to physically map the laser frequency comb into the velocity comb of the excited Rb atoms at room temperature. Upon resonant excitation by discrete optical frequencies the velocity distribution of the excited Rb atoms shows comblike structure. Simultaneously, velocity-selective population transfer occurs between ground-state hyperfine levels. Both facts are observed by modified direct frequency comb spectroscopy and verified by a detailed density matrix treatment of the multilevel system in resonant field.

DOI: 10.1103/PhysRevA.73.043407 PACS number(s): 32.80.Qk, 42.50.Gy

I. INTRODUCTION

The subject of the coherent interaction of atomic systems with long trains of laser pulses generated externally to the laser is more than 20 years old [1–3]. The frequency spectrum of the pulse train consists of a series of fringes separated by the pulse repetition rate [4]. The fringes are regular in frequency space if the pulses in the pulse train have a defined phase relation relative to each other. In the systems where the atomic coherence relaxation time is longer than the pulse repetition period the atoms interact with the spectrum of the pulse train, and not with the spectrum of a single pulse. In that account the short pulse trains can be used for the high-resolution spectroscopy, where the observed linewidths are much smaller than the Fourier-transform limit of the individual pulse in the train.

Ultrashort, mode-locked lasers have brought new insights into different physical phenomena [5]. Mode-locked, phase-stabilized femtosecond lasers with high-repetition rates produce stabilized wide-bandwidth optical frequency combs (regularly spaced series of sharp lines). The phase controlled wide-bandwidth optical frequency comb [6] can be referenced to the microwave cesium time standard, thereby providing a series of secondary reference lines that may be extended across the XUV [7] and optical spectrum [8]. This has enabled important advances in metrology [9], optical frequency synthesis [10] and measurements [11,12], optical atomic clocks [13], and coherent pulse synthesis and manipulation [14].

Recently, high-resolution comb spectroscopy of one- and two- photon transitions in laser-cooled and trapped rubidium atoms was reported [15–18]. The laser frequency comb is varied in these experiments. The one-photon signal is observed whenever one of the laser modes is resonant with a transition frequency of the system. In the case of the two-photon transitions the counterpropagating beams are used. There are several hundred thousand comb pairs that yield the same sum frequency contributing to the two-photon transition amplitude. The authors of Ref. [16] reported about a unification of the fs comb time and frequency domain. Direct frequency comb spectroscopy (DFCS) was developed, allowing simultaneous investigation of the time-resolved atomic dynamic and spectral probing in the frequency domain. In systems with relaxation times greater than the laser repetition period, the medium accumulates excitation in the form of coherence and excited-state population. The fs-pulse train effects in two- and three-level rubidium atoms were investigated experimentally and theoretically [19,20]. The necessity of considering accumulative effects for a full explanation of the coherent control signal obtained from the rubidium vapor was demonstrated [21].

In our recent paper [22] we presented an observation of the velocity-selective population transfer between the Rb ground-state hyperfine levels induced by fs-pulse train excitation. In present paper we extend our previous experimental investigation and present the theoretical treatment in more detail. We developed a modified DFCS which uses a fixed-frequency comb for the ^{85,87}Rb $5\,^2S_{1/2} \rightarrow 5\,^2P_{1/2,3/2}$ excitation and a weak cw scanning probe for ground levels population monitoring. The Rb ($5\,^2P_{1/2,3/2}$) excited atomic levels have relaxation times greater than the fs-laser repetition period. In the time domain this leads to population and coherence accumulation effects. This corresponds to the interaction of the Rb atoms with the fs-frequency comb in the frequency domain. As a result, velocity-selective excited-state hyperfine-level populations are obtained—i.e., the mapping of the frequency comb to the atomic velocity comb. Simultaneously, velocity-selective optical pumping of the ground hyperfine levels is achieved. We measured the ^{85,87}Rb ($5\,^2S_{1/2}$) hyperfine-level population by monitoring the $5\,^2S_{1/2} \rightarrow 5\,^2P_{3/2}$ probe laser absorption. Modulations in the $5\,^2S_{1/2} \rightarrow 5\,^2P_{3/2}$ hyperfine absorption line profiles are observed as a direct consequence of the velocity-selective optical pumping induced by the frequency comb excitation. The ^{85,87}Rb $5\,^2S_{1/2} \rightarrow 5\,^2P_{1/2,3/2}$ fs-pulse train excitation of a Doppler-broadened rubidium vapor was investigated theoretically in the context of the density-matrix formalism. Simulated $5\,^2S_{1/2} \rightarrow 5\,^2P_{3/2}$ absorption profiles were compared with the experiment, and the agreement was excellent. The dependence of the observed modulations upon the wavelength and power of the fs laser and external magnetic field was investigated experimentally.

II. EXPERIMENT

A simple experimental arrangement is shown in Fig. 1. In the experiment a Tsunami mode-locked Ti:sapphire laser

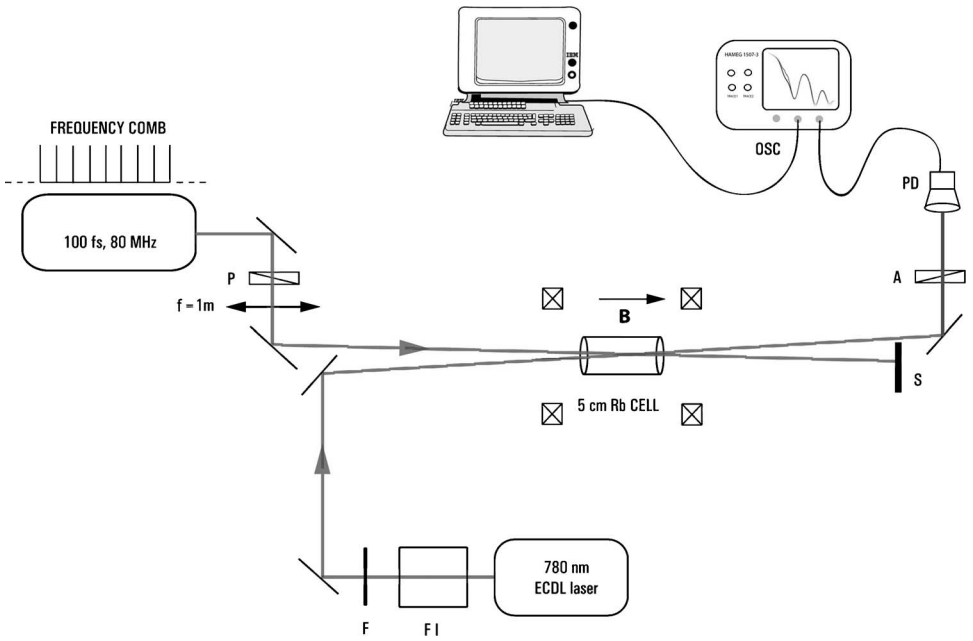

FIG. 1. Experimental scheme. PD: photodiode. P: polarizer. A: analyzer. FI: Faraday isolator. S: beam stopper. F: neutral density filter.

with pulse duration of ~100 fs and pulse repetition of 80 MHz was used. The frequency comb of the fs laser was kept fixed during the measurements. The output wavelength of the fs laser was positioned either at the Rb $5\,^2S_{1/2} \rightarrow 5\,^2P_{1/2}$ transition at 795 nm ($D1$ resonance line) or at Rb $5\,^2S_{1/2} \rightarrow 5\,^2P_{3/2}$ transition at 780 nm ($D2$ resonance line). The maximum average power used was up to 900 mW and a spectral full width at half maximum around 10 nm. It was focused onto the center of the glass cell containing rubidium vapor at room temperature with a $f=1$ m lens producing beam waist of about 300 μm. The cell was 5 cm long with an outer diameter of 2.5 cm. The homogeneous external magnetic field was generated with a pair of Helmholtz coils. The external magnetic field was orthogonal to the laser wave polarization and parallel to the laser propagation. The ^{85,87}Rb $5\,^2S_{1/2}$ hyperfine ground-state populations were probed with a weak cw diode laser (TOPTICA DL100, ECDL at 780 nm, output power ~2 μW/mm^2), which propagated nearly collinear with the fs laser, intersecting it under small angle in the center of the cell. The probe laser provided a continuous single-mode tuning range of up to 15 GHz, with a linewidth of the order of 1 MHz. Its frequency was scanned across the Doppler-broadened ^{85,87}Rb $5\,^2S_{1/2} \rightarrow 5\,^2P_{3/2}$ hyperfine transitions at a 0.3-GHz/ms scanning rate. The fs and probe lasers were linearly polarized perpendicular to each other. The transmission of the probe laser after passing through the cell was measured with a Hamamatsu Si photodiode, and the signal was fed into a digital oscilloscope (Tektronix TDS5104). The photodiode was placed at a distance of about 7 m from the cell in order to spatially separate fs and probe beams. Additionally, a linear analyzer was used.

III. THEORY

Theoretical modeling of the fs-pulse train interaction with the Rb atoms was carried out utilizing standard density-matrix analysis. In the case of $5\,^2S_{1/2} \rightarrow 5\,^2P_{1/2}$ fs excitation, four-level Rb atoms were considered, Fig. 2(a). The four-level atomic system comprises two $5\,^2S_{1/2}$ hyperfine ground levels ($F_g=2,3$ for ^{85}Rb and $F_g=1,2$ for ^{87}Rb) and two

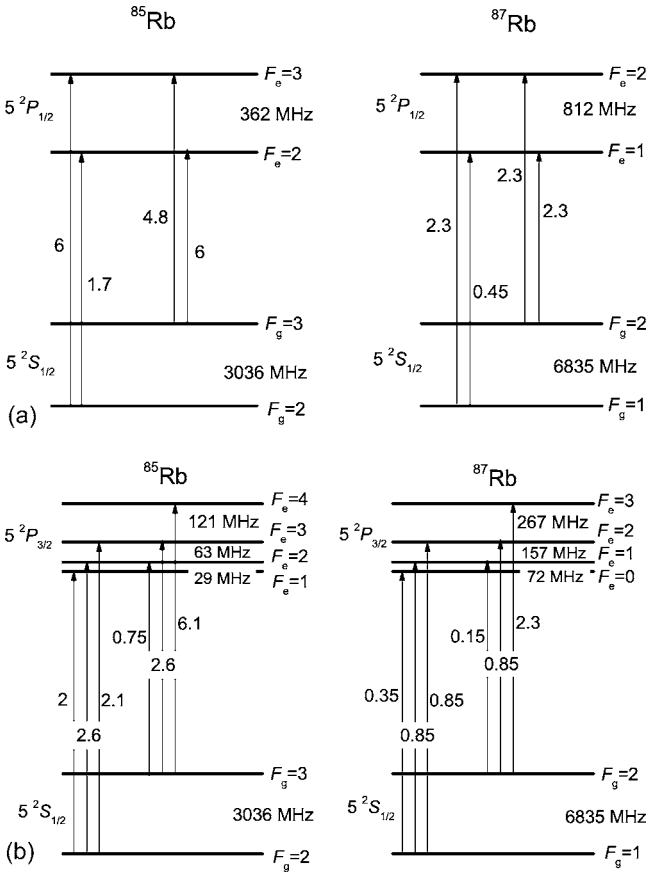

FIG. 2. Hyperfine energy schemes of the ^{85,87}Rb $5\,^2S_{1/2}$-$5\,^2P_{1/2}$four-level (a) and $5\,^2S_{1/2}$-$5\,^2P_{3/2}$ six-level (b) systems with the corresponding relative transition probabilities.

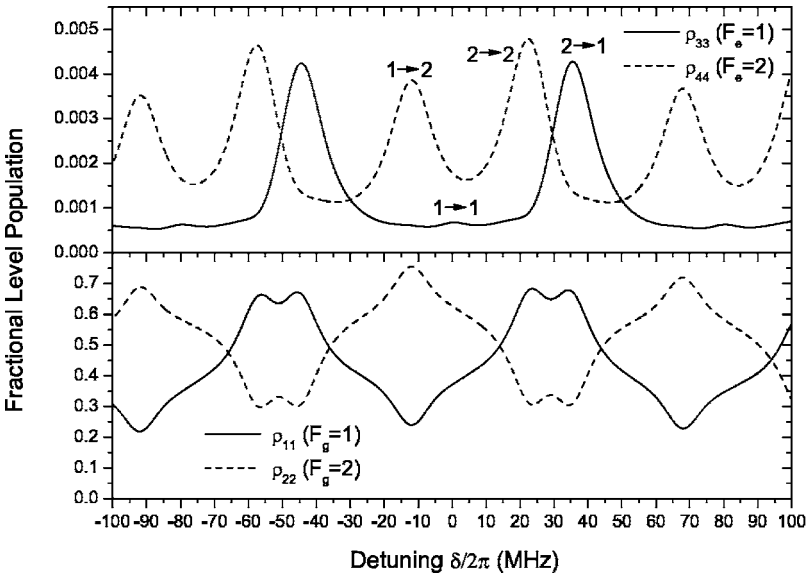

FIG. 3. ^{87}Rb calculated ground-(ρ_{11},ρ_{22}) and excited-(ρ_{33},ρ_{44}) state hyperfine-level populations for different atomic velocity groups in the case of $5\,^2S_{1/2}\rightarrow 5\,^2P_{1/2}$ fs-laser excitation (only a central part of the Doppler-broadened profile is presented).

$5\,^2P_{1/2}$ hyperfine excited levels ($F_e=2,3$ for ^{85}Rb and $F_e=1,2$ for ^{87}Rb). Our starting point is the Liouville equation for the density-matrix elements ρ_{kl} ($k,l=1,2,3,4$):

$$\frac{d\rho_{kl}}{dt} = -\frac{i}{\hbar}\langle k|[H,\rho]|l\rangle - \frac{1}{T_{kl}}\rho_{kl}, \tag{1}$$

where H is the Hamiltonian of the system and T_{kl} is the relaxation time of the ρ_{kl} density-matrix element. The Hamiltonian of the system is $H=H_0+H_{\text{int}}$, where H_0 is the Hamiltonian of the free atom and $(H_{\text{int}})_{kl}=-\mu_{kl}E_T(t)$ represents the interaction of the atom with the pulse train electric field. μ_{kl} is the dipole moment of the electronically allowed ($F_g\rightarrow F_e=F_g,F_g\pm 1$) transitions, extracted from Ref. [23]. The pulse train electric field is given by

$$E_T(t) = \left[\sum_{n=0}^{N}\varepsilon(t-nT_R)e^{in\Phi_R}\right]e^{i\omega_L t} = \varepsilon_T(t)e^{i\omega_L t}, \tag{2}$$

where N is a large integer (order of 10^6), $\varepsilon(t-nT_R)$ is the slowly varying envelope of the nth hyperbolic-secant laser pulse, Φ_R is the round-trip phase acquired by the laser within the cavity, T_R is the laser repetition period, and ω_L is the central laser angular frequency. $\varepsilon_T(t)$ is the slowly varying envelope of the pulse train. The pulse train frequency spectrum consists of a comb of N laser modes separated by $1/T_R$ and centered at $\omega_L+\Phi_R/T_R$. The nth-mode angular frequency is given by $\omega_n=\omega_L+\Phi_R/T_R\pm 2\pi n/T_R$.

From Eq. (1) a system of ten coupled differential equations for the slowly varying density-matrix elements was obtained. Additional terms were included in the equations to account for the repopulation of the ground states due to spontaneous decay from the excited states (repopulation terms) and thermalization of the hyperfine levels (collisional mixing term). The population of the kth atomic level is given by the diagonal density-matrix element ρ_{kk}, whereas off-diagonal elements σ_{kl}, where $\sigma_{kl}=\rho_{kl}e^{-i\omega_L t}$, represent the slowly varying envelope of the coherences. The equations for the slowly varying density-matrix elements are

$$\frac{d\rho_{11}}{dt} = \frac{i}{\hbar}(\sigma_{13}^*\mu_{13}\varepsilon_T + \sigma_{14}^*\mu_{14}\varepsilon_T - \sigma_{13}\mu_{13}\varepsilon_T^* - \sigma_{14}\mu_{14}\varepsilon_T^*) + \rho_{33}\Gamma_{31} + \rho_{44}\Gamma_{41} + \Pi(\rho_{22}-\rho_{11}), \tag{3a}$$

$$\frac{d\rho_{22}}{dt} = \frac{i}{\hbar}(\sigma_{23}^*\mu_{23}\varepsilon_T + \sigma_{24}^*\mu_{24}\varepsilon_T - \sigma_{23}\mu_{23}\varepsilon_T^* - \sigma_{24}\mu_{24}\varepsilon_T^*) + \rho_{33}\Gamma_{32} + \rho_{44}\Gamma_{42} + \Pi(\rho_{11}-\rho_{22}), \tag{3b}$$

$$\frac{d\rho_{33}}{dt} = \frac{i}{\hbar}(\sigma_{13}\mu_{13}\varepsilon_T^* + \sigma_{23}\mu_{23}\varepsilon_T^* - \sigma_{13}^*\mu_{13}\varepsilon_T - \sigma_{23}^*\mu_{23}\varepsilon_T) - \rho_{33}\Gamma_{31} - \rho_{33}\Gamma_{32} + \Pi(\rho_{44}-\rho_{33}), \tag{3c}$$

$$\frac{d\rho_{44}}{dt} = \frac{i}{\hbar}(\sigma_{14}\mu_{14}\varepsilon_T^* + \sigma_{24}\mu_{24}\varepsilon_T^* - \sigma_{14}^*\mu_{14}\varepsilon_T - \sigma_{24}^*\mu_{24}\varepsilon_T) - \rho_{44}\Gamma_{41} - \rho_{44}\Gamma_{42} + \Pi(\rho_{33}-\rho_{44}), \tag{3d}$$

$$\frac{d\sigma_{12}}{dt} = \frac{i}{\hbar}(\mu_{13}\varepsilon_T\sigma_{23}^* + \mu_{14}\varepsilon_T\sigma_{24} - \mu_{23}\varepsilon_T^*\sigma_{13} - \mu_{24}\varepsilon_T^*\sigma_{14}) + (i\omega_{12}-\gamma_{12})\sigma_{12}, \tag{3e}$$

$$\frac{d\sigma_{13}}{dt} = \frac{i}{\hbar}(\mu_{13}\varepsilon_T\rho_{33} + \mu_{14}\varepsilon_T\sigma_{34}^* - \mu_{13}\varepsilon_T\rho_{11} - \mu_{23}\varepsilon_T\sigma_{12}) + (i\omega_{13}-i\omega_L-\gamma_{13})\sigma_{13}, \tag{3f}$$

$$\frac{d\sigma_{14}}{dt} = \frac{i}{\hbar}(\mu_{13}\varepsilon_T\sigma_{34} + \mu_{14}\varepsilon_T\rho_{44}^* - \mu_{14}\varepsilon_T\rho_{11} - \mu_{24}\varepsilon_T\sigma_{12}) + (i\omega_{14}-i\omega_L-\gamma_{14})\sigma_{14}, \tag{3g}$$

$$\frac{d\sigma_{23}}{dt} = \frac{i}{\hbar}(\mu_{23}\varepsilon_T\rho_{33} + \mu_{24}\varepsilon_T\sigma_{34}^* - \mu_{13}\varepsilon_T\sigma_{12}^* - \mu_{23}\varepsilon_T\rho_{22}) + (i\omega_{13}-i\omega_{12}-i\omega_L-\gamma_{23})\sigma_{23}, \tag{3h}$$

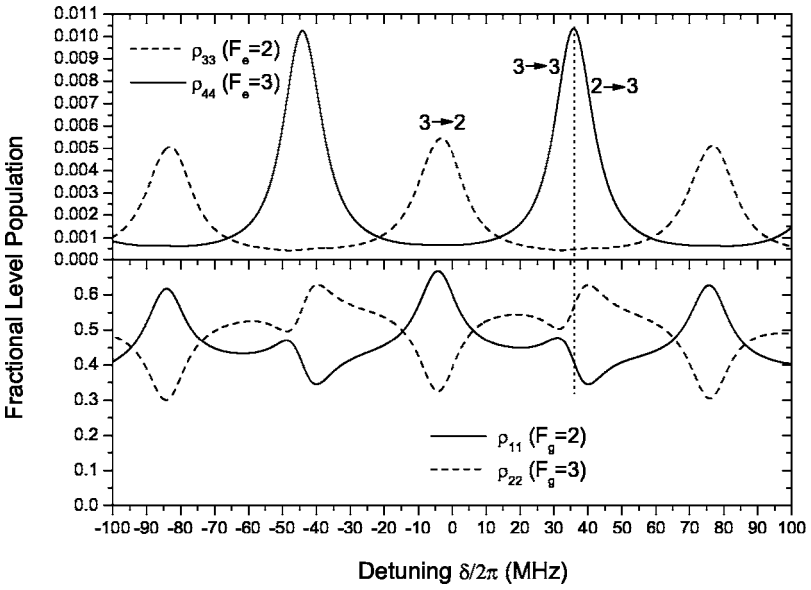

FIG. 4. ^{85}Rb calculated ground-(ρ_{11},ρ_{22}) and excited-(ρ_{33},ρ_{44}) state hyperfine-level populations for different atomic velocity groups in the case of $5\,^2S_{1/2}\rightarrow 5\,^2P_{1/2}$ fs-laser excitation (only a central part of the Doppler-broadened profile is presented).

$$\frac{d\sigma_{24}}{dt}=\frac{i}{\hbar}(\mu_{23}\varepsilon_T\sigma_{34}+\mu_{24}\varepsilon_T\rho_{44}-\mu_{14}\varepsilon_T\sigma_{12}^{*}-\mu_{24}\varepsilon_T\rho_{22})+(i\omega_{14}-i\omega_{12}-i\omega_L-\gamma_{24})\sigma_{24}, \tag{3i}$$

$$\frac{d\sigma_{34}}{dt}=\frac{i}{\hbar}(\mu_{13}\varepsilon_T^{*}\sigma_{14}+\mu_{23}\varepsilon_T^{*}\sigma_{24}-\mu_{14}\varepsilon_T\sigma_{13}^{*}-\mu_{24}\varepsilon_T\sigma_{23}^{*})+(i\omega_{14}-i\omega_{13}-\gamma_{34})\sigma_{34}. \tag{3j}$$

The subscripts refer to the four levels numbered from the lowest- to highest-energy state. $\omega_{kl}=(E_k-E_l)/\hbar$ where E_k and E_l are the energies of the appropriate atomic levels. Γ_{kl} and γ_{kl} are the population and coherence decay rates, respectively. Γ_{kl} were calculated from the $5\,^2P_{1/2}$ lifetime $T=27.7$ ns [24]. At low density vapor the $5\,^2P_{1/2}$ coherence lifetime is equal to $2T$ (55.4 ns). γ_{kl} coherence decay rates are calculated according to [25]

$$\gamma_{12}=\Pi, \tag{4a}$$

$$\gamma_{13}=\gamma_{23}=\frac{\Gamma_{31}}{2}+\frac{\Gamma_{32}}{2}+\Pi, \tag{4b}$$

$$\gamma_{14}=\gamma_{24}=\frac{\Gamma_{41}}{2}+\frac{\Gamma_{42}}{2}+\Pi, \tag{4c}$$

$$\gamma_{34}=\frac{\Gamma_{41}}{2}+\frac{\Gamma_{42}}{2}+\frac{\Gamma_{31}}{2}+\frac{\Gamma_{32}}{2}+\Pi, \tag{4d}$$

where Π is the collisional mixing term. It is included in the differential equations in order to allow the thermalization of the hyperfine states. In addition to the population transfer between two ground or two excited hyperfine states, this term contributes to the dephasing of coherences. It is given by the product of the collision cross section [26], the average

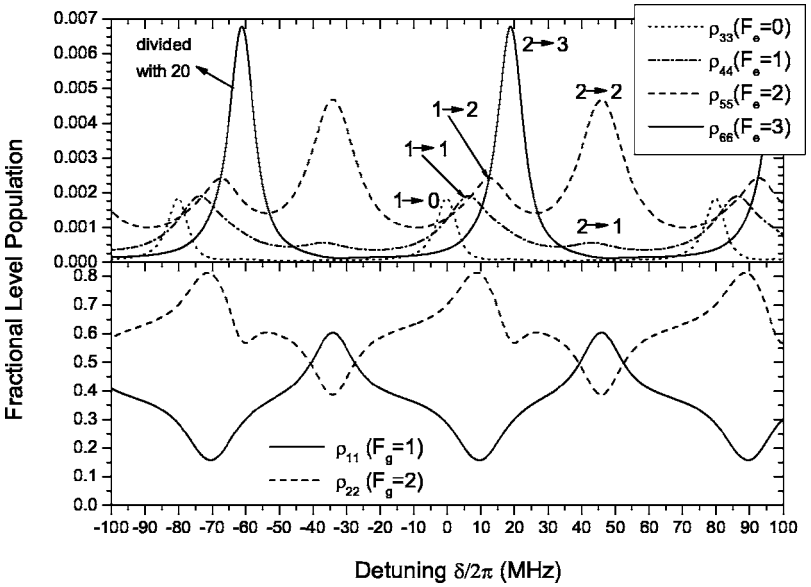

FIG. 5. ^{87}Rb calculated ground-(ρ_{11},ρ_{22}) and excited-$(\rho_{33},\rho_{44},\rho_{55},\rho_{66})$ state hyperfine-level populations for different atomic velocity groups in the case of $5\,^2S_{1/2}\rightarrow 5\,^2P_{3/2}$ fs-laser excitation (only a central part of the Doppler-broadened profile is presented).

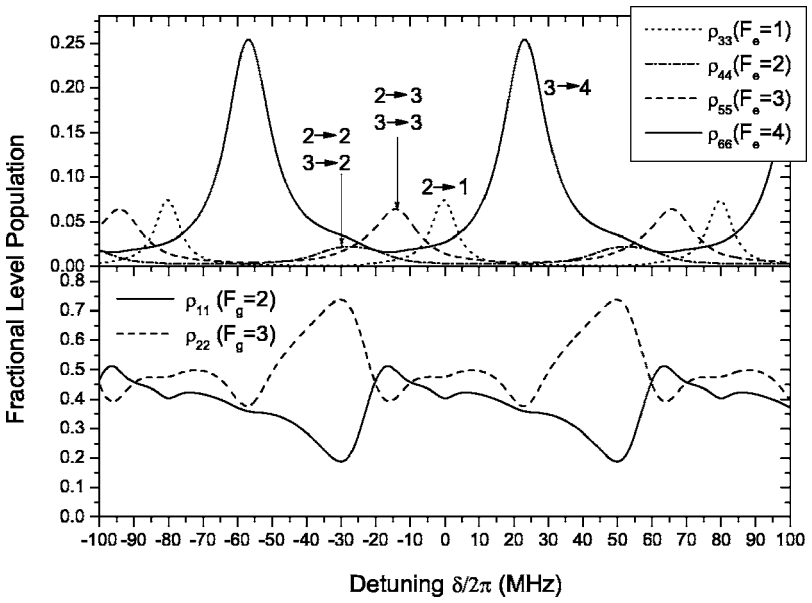

FIG. 6. ^{85}Rb calculated ground-(ρ_{11},ρ_{22}) and excited-$(\rho_{33},\rho_{44},\rho_{55},\rho_{66})$ state hyperfine-level populations for different atomic velocity groups in the case of $5\,^2S_{1/2}\rightarrow 5\,^2P_{3/2}$ fs-laser excitation (only a central part of the Doppler-broadened profile is presented).

atom velocity, and the atomic number density. In our experimental conditions it is about 8 kHz, which is three orders of magnitude smaller than the population and coherence relaxation rates. On that account the significant optical pumping of the ground hyperfine states can be achieved.

The system of differential equations (3a)–(3j) was integrated using a standard fourth-order Runge-Kutta method. The time evolutions of the atomic level populations and coherences were obtained. Due to the pulse repetition period T_R which is smaller than the relaxation times of the system, the system can never completely relax between two consecutive laser pulses. Therefore, the atoms accumulate excitation in the form of coherence and excited-state population [22].

The theoretical model used in the case of $5\,^2S_{1/2}\rightarrow 5\,^2P_{3/2}$ fs excitation is analogous to the one used for the $5\,^2S_{1/2}\rightarrow 5\,^2P_{1/2}$ fs excitation. The interaction of the fs pulse train with six-level Rb system was considered, Fig. 2(b). Six-level Rb system comprises two ground ($F_g=2,3$ for ^{85}Rb and $F_g=1,2$ for ^{87}Rb) and four excited ($F_e=1,2,3,4$ for ^{85}Rb and $F_e=0,1,2,3$ for ^{87}Rb) hyperfine levels. The six-level system is described by 21 coupled differential equations similar to Eqs. (3). The population and coherence decay rates were calculated from the $5\,^2P_{3/2}$ lifetime (26.24 ns) and coherence lifetime (52.48 ns) [24].

For the rubidium vapor at room temperature, the inhomogeneous Doppler broadening (of about 500 MHz) is significantly larger than the homogeneous broadening. Therefore, the atomic transition frequency ω_{ge} must be replaced with $\omega'_{ge}=\omega_{ge}+\vec{k}\cdot\vec{v}$, where $\vec{k}$ is the laser wave vector and $\vec{v}$ is the atomic velocity. Different velocity groups correspond to different detuning, $\delta=\vec{k}\cdot\vec{v}$, so for a given ω_n and a given $5\,^2S_{1/2}(F_g)\rightarrow 5\,^2P_{1/2}(F_e)$ hyperfine transition there is a velocity group (δ_n detuning), which fulfills $\omega_n=\omega'_{ge}$ resonance condition. Since the pulse train frequency spectrum consists of a comb of laser modes separated by $1/T_R$ (80 MHz), the resonance condition is also satisfied for the velocity groups with detuning $\delta=\delta_n\pm 2\pi k/T_R$, where k is positive integer. Therefore, different velocity groups are in different situation with

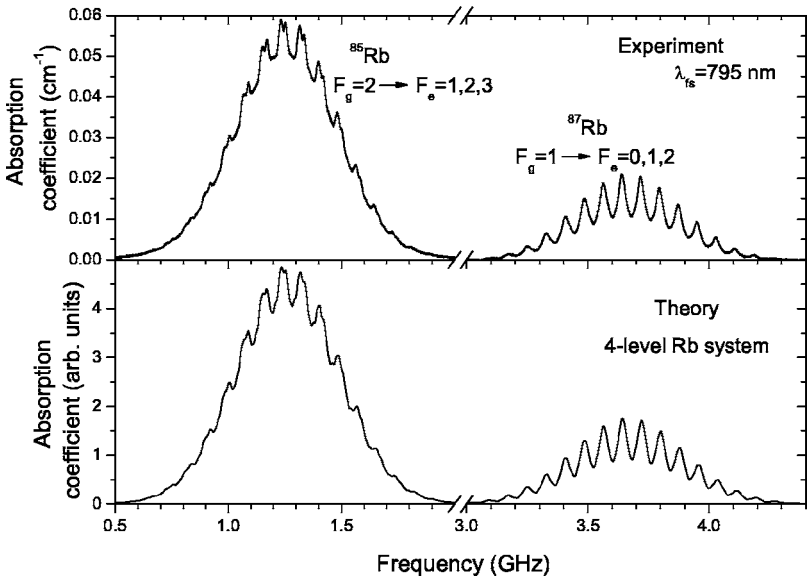

FIG. 7. The comparison of the measured and simulated ^{85,87}Rb $5\,^2S_{1/2}\rightarrow 5\,^2P_{3/2}$ hyperfine absorption line profiles in the case of $5\,^2S_{1/2}\rightarrow 5\,^2P_{1/2}$ fs-laser excitation.

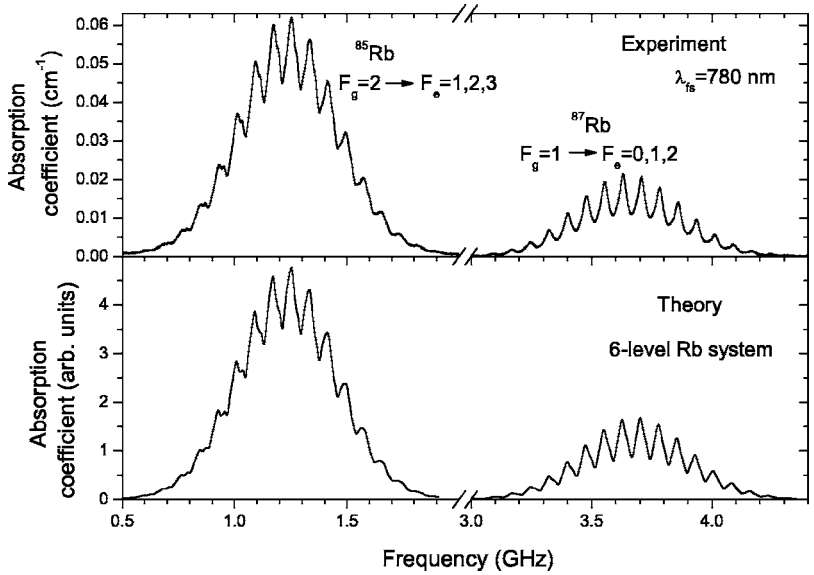

FIG. 8. The comparison of the measured and simulated ^{85,87}Rb $5\,^2S_{1/2} \rightarrow 5\,^2P_{3/2}$ hyperfine absorption line profiles in the case of $5\,^2S_{1/2} \rightarrow 5\,^2P_{3/2}$ fs-laser excitation.

respect to the excitation (accumulation) process, which leads to the velocity-selective optical pumping of ground hyperfine levels and velocity selective population in excited hyperfine levels.

IV. RESULTS

Calculated ^{85,87}Rb hyperfine ground- and excited-state levels populations for different atomic velocity groups (different detuning δ) in the case of $5\,^2S_{1/2} \rightarrow 5\,^2P_{1/2}$ and $5\,^2S_{1/2} \rightarrow 5\,^2P_{3/2}$ fs excitations are shown in Figs. 3–6. We present the level populations at time τ=1.25 μs instead of stationary-state solutions [22]. The time τ is the average interaction time of the atoms with the fs laser. It is calculated from the fs-laser beam diameter (300 μm) and most probable speed of the Rb atoms at room temperature. The fractional level populations are weighted by the Doppler profile (only a central part of the Doppler is presented). In the case of $5\,^2S_{1/2} \rightarrow 5\,^2P_{1/2}$ excitation, the calculations were performed for the electric field amplitude 1.5×10^6 V/m, T_R =12.5 ns, Φ_R=0, and ω_L equal to ^{87}Rb F_g=1 → F_e=2 and ^{85}Rb F_g=2 → F_e=3 transition frequencies. In the case of $5\,^2S_{1/2} \rightarrow 5\,^2P_{3/2}$ fs excitation, the electric field amplitude of 2×10^6 V/m, T_R=12.5 ns, Φ_R=0, and ω_L equal to ^{87}Rb F_g =1 → F_e=0, and ^{85}Rb F_g=2 → F_e=1 transition frequencies are used. The level populations exhibit unique oscillatory structure which varies with 80 MHz period. This is a direct consequence of the frequency comb. However, the level populations themselves are determined by the $5\,^2S_{1/2}$, $5\,^2P_{1/2}$, and $5\,^2P_{3/2}$ hyperfine energy splittings and relative transition probabilities. The optical pumping of the hyperfine ground levels and velocity-selective excitation—i.e., mapping of the frequency comb to the excited levels velocity comb—are clearly seen in Figs. 3–6.

In the case of $5\,^2S_{1/2} \rightarrow 5\,^2P_{1/2}$ excitation, the ^{87}Rb, F_g =1 (F_g=2) ground-state population in one period exhibits two maxima (minima) separated by 12 MHz and one minimum (maximum), Fig. 3. Two maxima in ρ_{11} come from

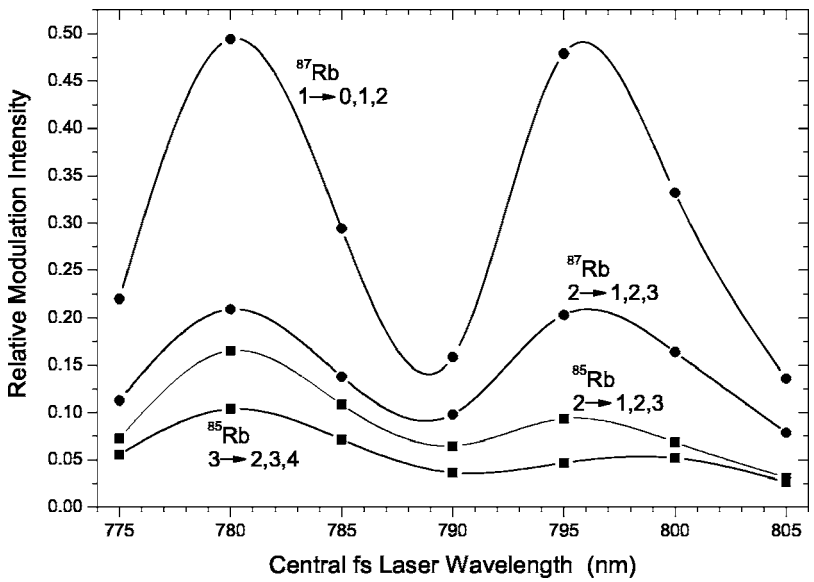

FIG. 9. Relative modulation intensities of four Rb absorption lines as a function of the central fs-laser wavelength.

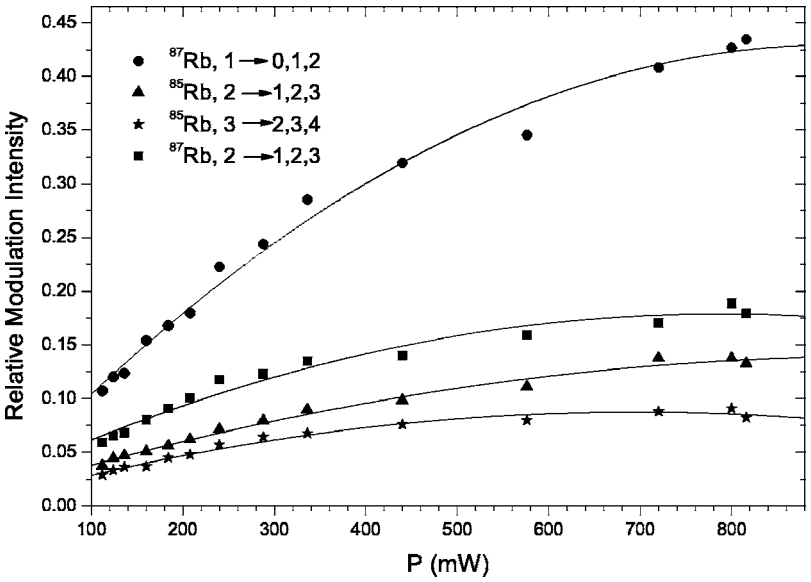

FIG. 10. Relative modulation intensity dependence on the fs-laser power, $5\,^2S_{1/2} \rightarrow 5\,^2P_{3/2}$ fs-laser excitation.

$F_g=2 \rightarrow F_e=1,2$ transitions, separated by 812 MHz. However, due to the 80-MHz laser mode separation in the comb spectrum, the resonance condition for these two transitions is obtained for $\delta=12$ MHz. The minimum in ρ_{11} corresponds to the $F_g=1 \rightarrow F_e=2$ transition. Due to the small relative transition probability of the $F_g=1 \rightarrow F_e=1$ transition, there is no significant optical pumping effect connected to this excitation. The $F_g=2$ ($F_g=3$) populations for ^{85}Rb, Fig. 4, exhibit in one-period two maxima (minima) and one minimum (maximum). The $5\,^2S_{1/2}$ hyperfine splitting is 3036 MHz, nearly a multiple of 80 MHz. Therefore, for one velocity group, when the laser is resonant with the $F_g=2 \rightarrow F_e=3$ transition (minimum in ρ_{11}), it is 4 MHz off-resonance with respect to the $F_g=3 \rightarrow F_e=3$ transition (smaller maximum in ρ_{11}). As a result, the contributions of two transitions are not resolved in the ρ_{44} level population. The second maximum in ρ_{11} comes from the $F_g=3 \rightarrow F_e=2$ transition, whereas the influence of the $F_g=2 \rightarrow F_e=2$ transition is not observed due to the small transition probability.

In the case of $5\,^2S_{1/2} \rightarrow 5\,^2P_{3/2}$ excitation, the ^{87}Rb, $F_g=1$ ground-level population in one period exhibits one maximum and one minimum, Fig. 5. The minimum comes as a result of the $F_g=1 \rightarrow F_e=1$ and $F_g=1 \rightarrow F_e=2$ hyperfine transitions, which are 3 MHz detuned with respect to the 80 MHz separation in the comb spectrum ($F_e=1$ and $F_e=2$ energy separation is 157 MHz). The maximum comes as a result of $F_g=2 \rightarrow F_e=1$ and $F_g=2 \rightarrow F_e=2$ hyperfine transitions. The $F_g=1,2 \rightarrow F_e=1,2$ transitions are optically open ones; therefore, they induce strong optical pumping of the ground hyperfine-level populations. When the resonant condition is fulfilled for one of these transitions, the minimum formed in ρ_{11} corresponds to the maximum in ρ_{22} and vice versa. $F_g=1 \rightarrow F_e=0$ and $F_g=2 \rightarrow F_e=3$ are optically closed transitions. $F_g=2 \rightarrow F_e=3$ hyperfine transition cause an additional minimum in ρ_{22} (smaller one) without a corresponding maximum in ρ_{11}. The $F_g=1 \rightarrow F_e=0$ transition does not lead to the second minimum in the ρ_{11} level population due to the small relative transition probability. The excited-level popu-

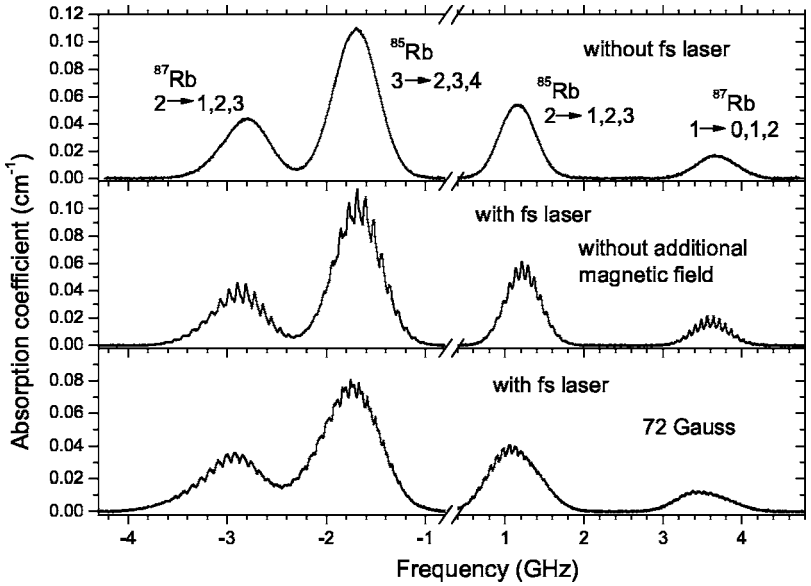

FIG. 11. Measured ^{85,87}Rb $5\,^2S_{1/2} \rightarrow 5\,^2P_{3/2}$ absorption spectra for $5\,^2S_{1/2} \rightarrow 5\,^2P_{3/2}$ fs-laser excitation in the conditions with and without an external magnetic field.

lations are below 1%, except for the $F_e=3$ level, which reaches a maximum value of about 14% due to the optically closed transition with a strong transition probability. In the case of ^{85}Rb, $F_g=2,3\rightarrow F_e=2,3$ are optically open transitions. These transitions cause strong optical pumping of ground hyperfine levels, so for each minimum (maximum) in ρ_{11} there is a corresponding maximum (minimum) in ρ_{22}, Fig. 6. Optically closed transitions $F_g=2\rightarrow F_e=1$ and $F_g=3\rightarrow F_e=4$ result in minima in ground-level populations without corresponding maxima. Due to the smaller $F_g=2\rightarrow F_e=1$ transition probability, the minimum in the ρ_{11} population is hardly discernable. The excited-level populations are above 5%. Again, due to the $F_g=3\rightarrow F_e=4$ strong optically closed transition, the $F_e=4$ level population reaches 25%.

From the discussion given above it is evident that the ^{85,87}Rb ground- and excited-state hyperfine-level populations are determined by the hyperfine energy splittings and relative transition probabilities with a periodic behavior given by the mode separation in the frequency comb.

The velocity-selective experimental observation of hyperfine ground-state populations is achieved by monitoring the weak cw probe laser transmission. The probe laser wavelength is continuously scanned across all four Doppler-broadened $5\,^2S_{1/2}\rightarrow 5\,^2P_{3/2}$ absorption lines at 780 nm. In the weak-field approximation (probe intensity $\sim 2\ \mu\mathrm{W/mm}^2$) and linear absorption regime, the measured optical thickness is directly proportional to the ρ_{11} and ρ_{22} hyperfine ground-level populations. By scanning the probe laser frequency, ^{85,87}Rb ($5\,^2S_{1/2}$) hyperfine populations of different velocity groups were probed. The absorption spectra consist of four profiles, two of them resulting from ^{85}Rb absorption (inner two) and the other two from ^{87}Rb (outer two). Two lines corresponding to each isotope are a result of the hyperfine splitting of the ground state, which is 3036 MHz (^{85}Rb) and 6835 MHz (^{87}Rb). The excited-state $5\,^2P_{3/2}$ hyperfine structure is not resolved due to the Doppler broadening. Therefore, each of the four absorption lines consists of three Doppler-broadened hyperfine transitions $[5\,^2S_{1/2}(F_g)\rightarrow 5\,^2P_{3/2}(F_e=F_g,F_g\pm 1)]$. As a result of the fs-pulse train interaction with rubidium atoms, the modulations in the absorption line profiles are observed in the measured probe laser absorption spectra. The modulations period of 80 MHz corresponds to the fs-pulse repetition rate.

In Figs. 7 and 8 we present the measured and simulated ^{87}Rb $F_g=1\rightarrow F_e=0,1,2$ and ^{85}Rb $F_g=2\rightarrow F_e=1,2,3$ absorption lines in the cases of $5\,^2S_{1/2}\rightarrow 5\,^2P_{1/2}$ and $5\,^2S_{1/2}\rightarrow 5\,^2P_{3/2}$ fs-laser excitations. Only parts of the absorption spectra are presented in order to improve visualization. The complete absorption spectra in the case of $^2S_{1/2}\rightarrow 5\,^2P_{1/2}$ fs excitation are given in our previous paper [22]. In the theoretical simulation of measured absorption spectra the ^{85,87}Rb ρ_{11} and ρ_{22} hyperfine ground-level populations shown in Figs. 3–6 were used. For each hyperfine transition, we calculated the convolution of the velocity distribution of the ground-state population with the Lorentzian profile of natural linewidth. One absorption line is calculated by adding the contributions of three hyperfine components [27]. The theoretical results show excellent agreement with the experiment. Changing the fs-laser excitation from $^2S_{1/2}\rightarrow 5\,^2P_{1/2}$ to $^2S_{1/2}\rightarrow 5\,^2P_{3/2}$ does not lead to a significant change in the modulations of ^{87}Rb absorption profiles. On the other hand, there is a significant change in both the intensity and shape of the modulations in the ^{85}Rb absorption profiles. Additionally, the modulations are stronger for ^{87}Rb. Modulations of up to 50% were observed for the ^{87}Rb $F_g=1\rightarrow F_e=0,1,2$ absorption line. Each profile is greatly affected by the excited-state hyperfine splittings since in the Doppler-broadened medium each absorption profile is a superposition of three hyperfine lines. If the frequency separation of three hyperfine lines forming an absorption line is favorable, as is the case for ^{87}Rb, the thus formed absorption line exhibits stronger modulations. Simultaneously, the shape of a hyperfine line is given by the velocity distribution of the ground level population, Figs. 3–6. The difference in the shape of absorption line modulations for ^{87}Rb and ^{85}Rb is therefore expected.

The relative modulation intensities of four Rb absorption lines are presented in Fig. 9 as a function of the central

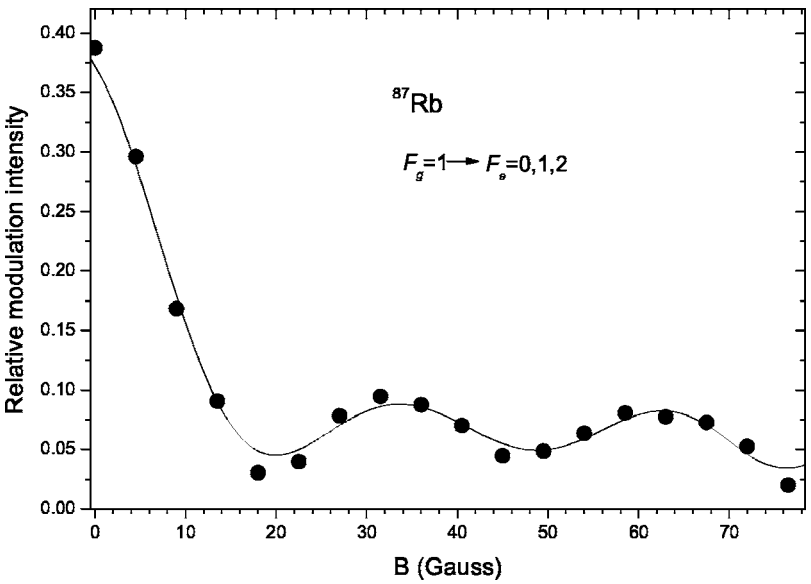

FIG. 12. Relative modulation intensity of ^{87}Rb $F_g=1\rightarrow F_e=0,1,2$ absorption line as a function of external magnetic field strength (dots). The solid line is an eye-guiding fit to the experimental data.

fs-laser wavelength. The relative modulation intensity is calculated as the ratio of the modulation amplitude and measured probe absorption without the fs laser. Two maxima corresponding to the $^2S_{1/2} \rightarrow 5\,^2P_{3/2}$ at 780 nm and $^2S_{1/2} \rightarrow 5\,^2P_{1/2}$ at 795-nm fs-laser excitation are clearly recognized.

The relative modulation intensity dependence on the fs-laser power is shown in Fig. 10. The shape of the modulations remains the same in the measured power range. The saturation of the modulation intensities is observed for the fs-laser power above 440 mW.

In order to investigate the dependence of the observed modulations on the energy-level pattern we applied an external magnetic field. In an external magnetic field the Rb ground- and excited-state levels are not characterized any more by the total angular momentum quantum numbers F_g and F_e, but they are a mixture of these states created by the external field. The magnetic sublevel energies are dependent on the external magnetic field strength. For very low field strengths each hyperfine level experiences a linear Zeeman effect. As the field strength increases, the Zeeman energy comes close to the hyperfine splitting energy and the energy-level pattern becomes complex. In our experimental geometry the optical transitions between hyperfine ground- and excited-state levels follow the $\Delta M = \pm 1$ selection rule. Measured absorption spectra for $5\,^2S_{1/2} \rightarrow 5\,^2P_{3/2}$ fs laser excitation with and without external magnetic field are shown in Fig. 11. In the external magnetic field the shape of the modulations changes, while the relative modulation intensity decreases. The relative modulation intensity dependence on external magnetic field for the ^{87}Rb $F_g = 1 \rightarrow F_e = 0,1,2$ absorption line shows damped oscillatory behavior with a period of about 30 G, as seen in Fig. 12. When the external field is applied this absorption line consists of 12 hyperfine Zeeman transitions. As previously discussed, the observed absorption line modulations strongly depend upon the energy-level splittings, transition probabilities, and fs-frequency comb spectrum. The influence of the ground- and excited-state energy-level structure is twofold: first, through the fs excitation process, which determines the ground-state level populations, and second, through the formation of the absorption line profile. For the field strength, which leads to favorable energy-level splittings (the frequency separation of different transitions is a multiple of 80 MHz), one would expect stronger modulations. Taking into account the complexity of the system it is hard to give any definite predictions about the modulations dependence on magnetic field strength. We expect that the modulations should be pronounced in the condition when the 5 $S_{1/2}$ atomic Larmor frequency is equal to (or a multiple of) the pulse repetition rate [3]. However, the first-order ground-state Zeeman coherence is at 110 G, which was out of our experimental magnetic field strength range. Measured ^{87}Rb $F_g = 1 \rightarrow F_e = 0,1,2$ absorption line profiles in the conditions without external magnetic field and with the magnetic field strengths of 18 G (first minimum of the modulation amplitude) and 36 G (second maximum of the modulation amplitude) are shown in Fig.13.

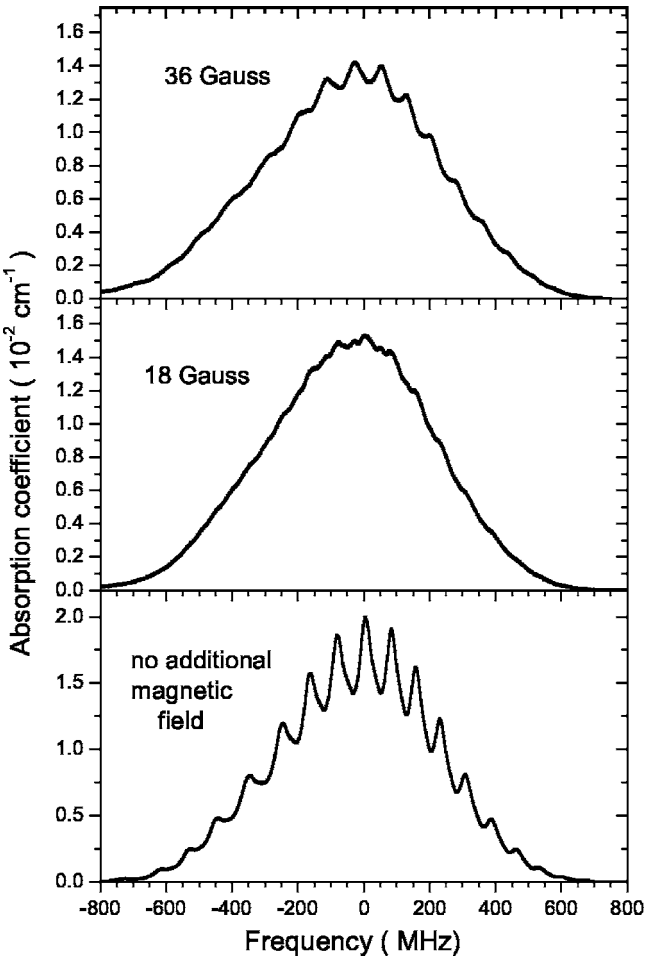

FIG. 13. Measured ^{87}Rb $F_g = 1 \rightarrow F_e = 0,1,2$ absorption line profiles in the conditions without an external magnetic field and with magnetic field strengths of 18 G (minimum in Fig. 12) and 36 G (maximum in Fig. 12).

V. CONCLUSION

We present as experimental and theoretical study of the resonant excitation of rubidium atoms with femtosecond-pulse train in the conditions when the pulse repetition period is shorter than the excited-state relaxation time. The velocity-selective optical pumping of the ground-state hyperfine levels and velocity-comb-like excited-state hyperfine-level populations are demonstrated. Both effects are a direct consequence of the fs-pulse train excitation considered in the frequency domain.

A simple experimental apparatus was employed to develop a modified direct-frequency comb spectroscopy which uses a fixed-frequency comb for the ^{85,87}Rb $5\,^2S_{1/2} \rightarrow 5\,^2P_{1/2,3/2}$ excitation and a highly monochromatic weak cw scanning probe for ground-level population monitoring. Excellent agreement is obtained with the theoretical model based on the density-matrix formalism of a multilevel atomic system excited by the fs-pulse train.

The coherent accumulation process through the excitation by a train of the fs pulses has been demonstrated. A recent work [28] on coherent effects describes the observation of the electromagnetically induced transparency (EIT) in Rb prepared by a comb of optical pulses produced by a cw mode-locked diode laser. We see a prospect of our work in an attempt to apply a femtosecond mode-locked laser to observe EIT resonances with possible applications in magne-

tometry [29], atomic clocks [13], and frequency chains [30].

In addition, this work shows that it is possible to directly manipulate the fractional populations of hyperfine ground-state levels by varying the comb optical frequency spectrum. This could lead to the interesting applications in the systems where Doppler broadening is negligible—for example, ultracold atoms and atomic beam experiments.

ACKNOWLEDGMENTS

We acknowledge support from the Ministry of Science and Technology of Republic of Croatia (Project No. 0035002), European Commission Research Training Network (FW-5), and Alexander von Humboldt Foundation (Germany).

[1] R. Teets, J. N. Eckstein, and T. W. Hänsch, Phys. Rev. Lett. **38**, 760 (1977).
[2] J. N. Eckstein, A. I. Ferguson, and T. W. Hänsch, Phys. Rev. Lett. **40**, 847 (1978).
[3] J. Mlynek, W. Lange, H. Harde, and H. Burggraf, Phys. Rev. A **24**, 1099 (1981).
[4] T. Udem, Science **307**, 364 (2005).
[5] A. H. Zewail, *Femtochemistry: Ultrafast Dynamics of the Chemical Bond* (World Scientific, Singapore, 1994).
[6] R. J. Jones, I. Thomann, and J. Ye, Phys. Rev. A **69**, 051803(R) (2004).
[7] R. J. Jones, K. D. Moll, M. J. Thorpe, and J. Ye, Phys. Rev. Lett. **94**, 193201 (2005).
[8] S. T. Cundiff and J. Ye, Rev. Mod. Phys. **75**, 325 (2003).
[9] S. Witte, R. Th. Zinkstok, W. Ubachs, W. Hogervorst, and K. S. E. Eikema, Science **307**, 400 (2005).
[10] A. Bartels, N. R. Newbury, I. Thomann, L. Hollberg, and S. A. Diddams, Opt. Lett. **29**, 403 (2004).
[11] Th. Udem, J. Reichert, R. Holzwarth, and T. W. Hänsch, Phys. Rev. Lett. **82**, 3568 (1999).
[12] M. Niering *et al.*, Phys. Rev. Lett. **84**, 5496 (2000).
[13] S. A. Diddams *et al.*, Science **293**, 825 (2001).
[14] R. K. Shelton *et al.*, Science **293**, 1286 (2001).
[15] M. J. Snadden, A. S. Bell, E. Riis, and A. I. Ferguson, Opt. Commun. **125**, 70 (1996).
[16] A. Marian, M. C. Stowe, J. R. Lawall, D. Felinto, and J. Ye, Science **306**, 2063 (2004).
[17] H.-C. Chui, M.-S. Ko, Y.-W. Liu, and J.-T. Shy, Opt. Lett. **30**, 842 (2005).
[18] A. Marian, M. C. Stowe, D. Felinto, and J. Ye, Phys. Rev. Lett. **95**, 023001 (2005).
[19] D. Felinto, C. A. C. Bosco, L. H. Acioli, and S. S. Vianna, Opt. Commun. **215**, 69 (2003).
[20] D. Felinto, L. H. Acioli, and S. S. Vianna, Phys. Rev. A **70**, 043403 (2004).
[21] D. Felinto, C. A. C. Bosco, L. H. Acioli, and S. S. Vianna, Phys. Rev. A **64**, 063413 (2001).
[22] D. Aumiler, T. Ban, H. Skenderović, and G. Pichler, Phys. Rev. Lett. **95**, 233001 (2005).
[23] D. A. Steck, Rubidium 87 D Line Data, http://steck.us/alkalidata
[24] U. Volz and H. Schmoranzer, Phys. Scr. **T65**, 48 (1996).
[25] J. R. Boon, E. Zekou, D. J. Fulton, and M. H. Dunn, Phys. Rev. A **57**, 1323 (1998).
[26] C. Cohen-Tannondji and A. Kastler, Prog. Opt. **5**, 3 (1966).
[27] D. Aumiler, T. Ban, and G. Pichler, Phys. Rev. A **70**, 032723 (2004).
[28] V. A. Sautenkov *et al.*, Phys. Rev. A **71**, 063804 (2005).
[29] M. O. Scully, Phys. Rev. Lett. **67**, 1855 (1991).
[30] S. A. Diddams, D. J. Jones, J. Ye, S. T. Cundiff, and J. L. Hall, Phys. Rev. Lett. **84**, 5102 (2000).